

Topological defects and inhomogeneous spin patterns induced by the quadratic Zeeman effect in spin-1 Bose-Einstein condensates

Dun Zhao,^{1,2,3} Shu-Wei Song,² Lin Wen,² Zai-Dong Li,⁴ Hong-Gang Luo,^{3,5} and Wu-Ming Liu²

¹*School of Mathematics and Statistics, Lanzhou University, Lanzhou 730000, China*

²*Beijing National Laboratory for Condensed Matter Physics, Institute of Physics, Chinese Academy of Sciences, Beijing 100190, China*

³*Center for Interdisciplinary Studies, Lanzhou University, Lanzhou 730000, China*

⁴*Hebei University of Technology, Tianjin 300401, China*

⁵*Beijing Computational Science Research Center, Beijing 100084, China*

(Received 22 September 2013; revised manuscript received 6 August 2014; published 20 January 2015)

We obtain analytically two kinds of inhomogeneous spin domain configurations endowed with time-dependent periodic domain walls in spin-1 Bose-Einstein condensate, which result from the positive and negative quadratic Zeeman effects, respectively. It is shown analytically that the topological defects are given by the unmagnetized atoms, at which the order parameter is of polar phase, but besides them, the order parameter is of axisymmetry-broken phase. The quadratic Zeeman effect can be tuned to induce the dynamical phase transition of the spin domain, and its sign can affect the topological structure of the spin pattern. These features arise from the axisymmetry breaking due to the pointwise-different population exchange between the sublevels determined uniquely by the quadratic Zeeman effects. The related experimental observations for the spin-1 ⁸⁷Rb and ²³Na condensates are also discussed.

DOI: [10.1103/PhysRevA.91.013619](https://doi.org/10.1103/PhysRevA.91.013619)

PACS number(s): 67.85.-d, 03.75.Lm, 03.75.Mn, 05.30.Rt

I. INTRODUCTION

The realization of spinor Bose-Einstein condensate (BEC) in an optical trap [1–4] provides a unique system in which to study rich quantum phenomena [5–17]. While BEC in a magnetic trapping can be controlled precisely by many techniques, such as Feshbach resonance and dispersion management [18–23], the spinor BEC can be controlled by tuning the spin-exchange interaction via optical [24,25] or microwave [26] Feshbach resonance techniques. However, a powerful way to control the spinor BEC is to use the quadratic Zeeman effect, which results from the Zeeman energy difference in a spin-flip collision between different hyperfine levels. It not only leads to rich novel ground states and spin structures [27–32], but also significantly affects spin dynamics [33–41], phase transitions [41,42], symmetry [15,43], and the vortex state [44].

In spinor BEC under an external magnetic field B , the quadratic Zeeman effect is proportional to B^2 . Because of its competition with the spin-exchange interaction, the quadratic Zeeman effect becomes a key factor in determining the properties of the spinor gas. Experimentally, the quadratic Zeeman effect is tunable and its sign can be varied to be either positive or negative [4,15,30,40,45]. By use of the quadratic Zeeman effect, the single-particle energies can be varied to control the dynamical instabilities induced by the spin mixing collisions; these instabilities provide a great chance to access to a rich variety of physical phenomena. Although many exciting features of spinor BEC under quadratic Zeeman effect have been investigated, it is still not very clear how the quadratic Zeeman effect influences the spin dynamics, especially when the quadratic Zeeman effect is negative [4].

In this paper, we obtain the exact solutions for the spin-1 BEC in the presence of linear and quadratic Zeeman effects. We show that the quadratic Zeeman effect can give rise to pointwise-different population exchange between the sublevels of spin-1 BEC, which leads to the axisymmetry breaking, and brings on the time- and space-dependent magnetization. We describe in detail two novel kinds of

inhomogeneous spin patterns, which possess periodic spin domain walls (DWs) formed by the topological defects that are constituted by the zero-population-transfer areas, due to the positive and negative quadratic Zeeman effect, respectively. The quadratic Zeeman effect also deeply affects the topological structure of the spin patterns. Furthermore, for a positive quadratic Zeeman effect, the features of the spin domain described by the exact solution are in agreement with the experimental observation in [3] for a spin-1 ⁸⁷Rb Bose gas; for a negative quadratic Zeeman effect, it gives a theoretical supplement for the experiment of ²³Na reported in [4]. Our results provide a perspective on the controllability of spinor BEC via the quadratic Zeeman effect.

II. THE MODEL AND METHOD

In this paper, we only deal with the spatially homogeneous (the external trap $V_{\text{trap}} = 0$) spin-1 BEC. Up to now, BEC experiments are all carried out in atomic traps; however, as pointed out in Ref. [46], the results obtained from a homogeneous system may serve to provide primary estimates for certain physical quantities of a trapped BEC. Specifically, in the WKB semiclassical approximation, the homogeneous results are directly used to determine the spectrum of elementary excitations, which is then exploited to calculate various thermodynamic quantities. Moreover, there have been attempts to realize a homogeneous Bose-Einstein condensate [47,48]. For spatially homogeneous spin-1 BEC, under mean-field theory, in consideration of the Zeeman effect, the quasi-one-dimensional (1D) dynamics is governed by the Gross-Pitaevskii equations in dimensionless form [49,50]:

$$\begin{aligned}
 i\partial_t \Phi_{\pm 1} &= -\frac{1}{2}\partial_x^2 \Phi_{\pm 1} + (c_0 + c_1)(|\Phi_{\pm 1}|^2 + |\Phi_0|^2)\Phi_{\pm 1} \\
 &\quad + (c_0 - c_1)|\Phi_{\mp 1}|^2\Phi_{\pm 1} + c_1\Phi_{\mp 1}^*\Phi_0^2 + (q \mp p)\Phi_{\pm 1}, \\
 i\partial_t \Phi_0 &= -\frac{1}{2}\partial_x^2 \Phi_0 + (c_0 + c_1)(|\Phi_1|^2 + |\Phi_{-1}|^2)\Phi_0 \\
 &\quad + 2c_1\Phi_0^*\Phi_1\Phi_{-1} + c_0|\Phi_0|^2\Phi_0,
 \end{aligned} \tag{1}$$

where $c_0 = \bar{c}_0/\bar{c}_1, c_1 = \pm 1$. Here the constant $p = \bar{p}/\bar{c}_1 n$ denotes the linear Zeeman effect, the constant $q = \bar{q}/\bar{c}_1 n$ denotes the quadratic Zeeman effect, $\bar{c}_0 = (g_0 + 2g_2)/3$ and $\bar{c}_1 = (g_2 - g_0)/3$ denotes effective constants of the mean-field and spin-exchange interaction, respectively [5,16], with the effective 1D couplings,

$$g_F = \frac{4\hbar^2 a_F}{M a_\perp^2} \frac{1}{1 - C a_F/a_\perp}.$$

Here a_F are the s -wave scattering lengths in the total hyperfine spin $F = 0, 2$ channel; a_\perp is the size of the transverse ground states; M is the atomic mass; $C = 1.4603 \dots$, n is the average particle density; and $\bar{p} = -g\mu_B B$ is the sum of the linear Zeeman energy, with g the Lande factor, B the external magnetic field that is assumed to be applied in the z direction, $\mu_B = e\hbar/2m_e$ (m_e is the electron mass, and $e > 0$ is the elementary charge) is the Bohr magneton, and $\bar{q} = \frac{(g\mu_B B)^2}{E_{hF}}$ is the quadratic Zeeman energy with the hyperfine splitting $E_{hF} = E_m - E_i$ given by the difference between the initial E_i and intermediate E_m energies. In addition, time t , position x , and $\Phi_{\pm 1,0}$ are in units of $\hbar/(|\bar{c}_1|n), \hbar/\sqrt{2M|\bar{c}_1|n}$ and $1/\sqrt{n}$, respectively. The interaction is ferromagnetic if $\bar{c}_1 < 0$ (such as ^{87}Rb) or antiferromagnetic if $\bar{c}_1 > 0$ (such as ^{23}Na). The value of \bar{q} can be tuned in the negative direction by using a linearly polarized microwave field due to the ac Stark shift, and \bar{c}_0 must be non-negative to avoid the collapse. Specifically, for ^{87}Rb , $c_0 = 216, c_1 = -1$; for ^{23}Na , $c_0 = 32, c_1 = 1$. Typically, for ^{87}Rb and ^{23}Na , $n \sim 10^{20} \text{ m}^{-3}$ [1,3,51], and $|\bar{c}_1|n \sim h \times 3.6 \text{ Hz}$ or $h \times 24.1 \text{ Hz}$. The time and length are measured in units of 10^{-2} s and 10^{-6} m , respectively.

In experiments, the linear Zeeman effect can be changed independently by applying a field gradient B' along the axis of the trapped condensate [1], taken as $B'z_b$ where z_b is the gradient field range. The quadratic Zeeman effect can be changed independently by applying a weak external bias field B [1], which is given by $\bar{q} = \hat{q}B^2$. It is found that $\hat{q} = 71.65 \text{ Hz G}^{-2}$ for ^{87}Rb and 278 Hz G^{-2} for ^{23}Na [1]. In general, under a bias field, for spin-1 ^{23}Na or ^{87}Rb BEC, we have $q > 0$. However, by using ac Stark shift induced by a microwave dressing field, $q < 0$ is still accessible [4,45]. The controllability of the sign and its magnitude of the quadratic Zeeman effect provides a powerful way to manipulate spinor BEC.

Our discussion is based on the analytical solutions of Eq. (1). As Eq. (1) is derived from mean-field theory with zero temperature, our results only provide spin configurations in the sense of a thermodynamic equilibrium state. Although some simplifications [41] or approximations [52–56] have been made and some efficient analytical methods have been introduced [50,57–60], in the presence of the quadratic Zeeman effect, it seems that no analytical result has been reported. Even in the absence of the quadratic Zeeman effect, only some special cases of Eq. (1) have been studied analytically by a few authors. For example, in [58,59], the integrable models with the choice of the coupling constant $c_0 = c_1 = c (< 0 \text{ or } > 0)$ have been investigated; in [50,60], the order parameters were presented analytically by assuming $|\Phi_1| = |\Phi_{-1}|$. But these kinds of solutions cannot describe the spontaneous magnetization. In this paper, we deal with a

very general case, no assumption on c_0, c_1 is adopted, and in the solutions, $|\Phi_1| \neq |\Phi_{-1}|$, so these solutions can describe the spontaneous magnetization. We find that the uniform quadratic Zeeman effects can give rise to time-dependent topological defects which form the moving domain walls. It seems that such a phenomenon has not yet been reported in spinor BEC.

By a direct ansatz with Jacobian elliptic functions, we get two novel kinds of analytical solutions corresponding to a positive and negative quadratic Zeeman effect, respectively. To find explicit solutions of (1), we assume

$$\Phi_m(x, t) = r_m(x, t) e^{i\chi_m(x, t)} \quad (m = 1, 0, -1), \quad (2)$$

with the ansatz

$$\begin{aligned} r_m(x, t) &= A_m \text{sn}(\xi, \lambda) + B_m \text{cn}(\xi, \lambda) + C_m \text{dn}(\xi, \lambda), \\ \chi_{\pm 1}(x, t) &= k_{\pm 1}x - \mu_{\pm 1}t, \\ \chi_0(x, t) &= [\chi_1(x, t) + \chi_{-1}(x, t)]/2, \end{aligned}$$

where $\xi = kx + \omega t, A_m, B_m, C_m, k_{\pm 1}, \mu_{\pm 1}, k, \omega$ are parameters to be determined, $\text{sn}(\cdot, \lambda), \text{cn}(\cdot, \lambda)$ and $\text{dn}(\cdot, \lambda)$ are the real Jacobian elliptical functions [61], in which $\lambda^2 \leq 1$ gives the elliptic modulus, which determines the period of the functions. Denote by $K(\lambda) = \int_0^{\frac{\pi}{2}} \frac{d\theta}{\sqrt{1-\lambda^2 \sin^2(\theta)}}$, then the periods of $\text{sn}(\eta, \lambda), \text{cn}(\eta, \lambda)$, and $\text{dn}(\eta, \lambda)$ are $4K(\lambda), 4K(\lambda)$, and $2K(\lambda)$, respectively. Furthermore, the definition of these functions can be extended for $\lambda^2 > 1$ [62] by means of

$$\begin{aligned} \text{sn}(\eta, \lambda) &= 1/\lambda \text{sn}(\lambda\eta, 1/\lambda), \\ \text{cn}(\eta, \lambda) &= \text{dn}(\lambda\eta, 1/\lambda), \\ \text{dn}(\eta, \lambda) &= \text{cn}(\lambda\eta, 1/\lambda), \end{aligned} \quad (3)$$

so we think that λ is defined on the whole real line.

The Jacobian elliptical functions have the following properties:

$$\begin{aligned} \text{sn}(x, 0) &= \sin(x), \quad \text{cn}(x, 0) = \cos(x), \\ \text{dn}(x, 0) &= 1, \quad \text{sn}(x, 1) = \tanh(x), \\ \text{cn}(x, 1) &= \text{sech}(x), \quad \text{dn}(x, 1) = \text{sech}(x), \\ \text{sn}(x, \lambda)^2 + \text{cn}(x, \lambda)^2 &= 1, \\ \text{dn}(x, \lambda)^2 + \lambda^2 \text{sn}(x, \lambda)^2 &= 1. \end{aligned}$$

We see that the soliton form is a special case of a Jacobian elliptical function corresponding to $\lambda = 1$. In addition, the derivation operation is closed between the functions sn, cn , and dn as shown below:

$$\begin{aligned} \frac{d}{dx} \text{sn}(x, \lambda) &= \text{cn}(x, \lambda) \text{dn}(x, \lambda), \\ \frac{d}{dx} \text{cn}(x, \lambda) &= -\text{sn}(x, \lambda) \text{dn}(x, \lambda), \\ \frac{d}{dx} \text{dn}(x, \lambda) &= -\lambda^2 \text{sn}(x, \lambda) \text{cn}(x, \lambda). \end{aligned}$$

Substituting the ansatz (2) into (1) and using the above identities, we obtain polynomials in sn, cn , and dn . Setting the coefficients of the polynomials to be zeros, we get a system of algebraic equations on the unknown parameters A_m, B_m, C_m and $k_{\pm 1}, \mu_{\pm 1}, k, \omega$. This algebraic system can be solved, and we obtain our solutions. In fact, this procedure can provide

many interesting solutions for the spin-1 system, but in this paper we only care about the solutions with nonzero quadratic Zeeman effects.

We remark that our method can also be used to solve many other nonlinear partial differential equations.

III. TOPOLOGICAL DEFECTS AND INHOMOGENEOUS SPIN BY A POSITIVE QUADRATIC ZEEMAN EFFECT

For the positive quadratic Zeeman effect, we get an exact solution of (1) only under the ferromagnetic interaction, i.e., $c_1 = -1$ (we still use the symbol c_1 in the solution in order to emphasize its role) with the conditions $|c_1| < c_0$, which reads

$$\begin{aligned}\Phi_{\pm 1} &= \left[\sqrt{-c_1/(c_0 - c_1)} \operatorname{sn}(\xi, \lambda) \mp \frac{1}{2} \sqrt{-q/c_1} \operatorname{dn}(\xi, \lambda) \right] e^{i\chi_{\pm 1}}, \\ \Phi_0 &= \operatorname{sn}(\xi, \lambda) e^{i\chi_0},\end{aligned}\quad (4)$$

where $\xi = \sqrt{2q}(x - k_1 t)$, $\lambda = \sqrt{-2c_1/(q\delta)}$, and $\chi_{\pm 1} = k_1 x - \mu_{\pm 1} t$ with $\mu_{\pm 1} = k_1^2/2 - q(c_0 - 2c_1)/(2c_1) - 2c_1/\delta \mp p$, $2\chi_0 = \chi_1 + \chi_{-1}$, and $\delta = (c_0 - c_1)/(c_0 + c_1)$. Here k_1 is a free constant, which denotes the wave number of Φ_{+1} , and here is also the wave velocity of our traveling wave. For ^{87}Rb , $c_1 \ll c_0$, so we have $\Phi_{\pm 1} \approx \mp \frac{1}{2} \sqrt{-q/c_1} \operatorname{dn}(\xi, \lambda) e^{i\chi_{\pm 1}}$, which means that the density distribution of the $m_F = \pm 1$ components are almost the same. Obviously, in this solution, $q = 0$ is not permitted. This implies that such a solution can only exist in the presence of positive quadratic Zeeman effect; thus the initial components should be prepared under positive quadratic Zeeman effect. Theoretically, for (4), no initial conditions before the quadratic Zeeman effect exist.

When $t = 0$, (4) gives the initial state

$$\begin{aligned}\Phi_{\pm 1} &= \left[\sqrt{-c_1/(c_0 - c_1)} \operatorname{sn}(\sqrt{2q}x, \lambda) \right. \\ &\quad \left. \mp \frac{1}{2} \sqrt{-q/c_1} \operatorname{dn}(\sqrt{2q}x, \lambda) \right] e^{ik_1 x}, \\ \Phi_0 &= \operatorname{sn}(\sqrt{2q}x, \lambda) e^{ik_1 x},\end{aligned}\quad (5)$$

which presents a periodic density distribution if $q \neq 2/\delta$ ($\lambda \neq 1$), as shown in Fig. 1(a). When $q = 2/\delta$ ($\lambda = 1$), the

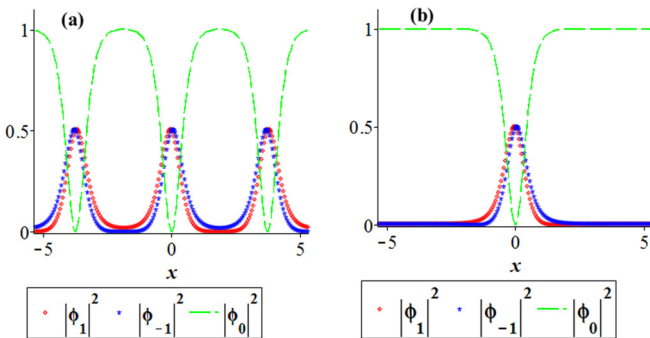


FIG. 1. (Color online) Initial states of $\Phi_{\pm 1}, \Phi_0$ given by (5) for ^{87}Rb : (a) $q = 2$, the periodic case; (b) $q = \frac{430}{217}$ ($\lambda = 1$), the soliton case. The other parameters are $p = 1$, $c_0 = 216$, $c_1 = -1$, $k_1 = 1$, $x \in [-5, 5]$. Such initial states should be prepared in the presence of positive quadratic Zeeman effect. Take $n = 2.8 \times 10^{20} \text{ m}^{-3}$, then $p = 1$ corresponds to $\bar{p} = 10.02 \text{ Hz}$; $q = 2$ corresponds to $\bar{q} = 20.05 \text{ Hz}$; and $q = \frac{430}{217}$ corresponds to $\bar{q} = 19.86 \text{ Hz}$.

density distribution becomes soliton type,

$$\begin{aligned}\Phi_{\pm 1} &= \left[\sqrt{-c_1/(c_0 - c_1)} \tanh(\sqrt{2q}x) \right. \\ &\quad \left. \mp \frac{1}{2} \sqrt{-q/c_1} \operatorname{sech}(\sqrt{2q}x) \right] e^{ik_1 x}, \\ \Phi_0 &= \tanh(\sqrt{2q}x) e^{ik_1 x}.\end{aligned}\quad (6)$$

as shown in Fig. 1(b).

Solution (4) reveals many interesting features of the spin domain configuration induced by the positive quadratic Zeeman effect. It is known that the spin dynamics can be described by the spin density vector $F = \{F_x, F_y, F_z\}$ [16], where F_z is the longitudinal magnetization parallel to the external magnetic field which describes the net magnetization, and $F_{\perp} = \{F_x, F_y\}$ indicates the transverse magnetization vector, which drives the atom exchange. The spin vector F is defined by

$$\begin{aligned}F_x &= \frac{1}{\sqrt{2}} [\Phi_1^* \Phi_0 + \Phi_0^* (\Phi_1 + \Phi_{-1}) + \Phi_{-1}^* \Phi_0], \\ F_y &= \frac{i}{\sqrt{2}} [-\Phi_1^* \Phi_0 + \Phi_0^* (\Phi_1 - \Phi_{-1}) + \Phi_{-1}^* \Phi_0], \\ F_z &= |\Phi_1|^2 - |\Phi_{-1}|^2.\end{aligned}$$

It is known that $|F_{\perp}| = \sqrt{F_x^2 + F_y^2}$ and $|F_z|$ determine the population exchange and the net magnetization, respectively. For solution (4), we have

$$\begin{aligned}F_x &= |F_{\perp}| \cos(pt), \quad F_y = -|F_{\perp}| \sin(pt), \\ F_z &= 2\sqrt{q/(c_0 - c_1)} \operatorname{sn}(\xi, \lambda) \operatorname{dn}(\xi, \lambda),\end{aligned}\quad (7)$$

where $|F_{\perp}| = \sqrt{-8c_1/(c_0 - c_1)} \operatorname{sn}^2(\xi, \lambda)$. Notice that when $\operatorname{sn}(\xi, \lambda) = 0$, we have $F_x = F_y = F_z = 0$, so all the zeros of $\operatorname{sn}(\xi, \lambda)$ provide the zeros of F . Usually, for system (1), in the absence of the quadratic Zeeman effect, F always has no zero and can be normalized, and thus the total magnetization density is conserved. In comparison, for solution (4), due to the zeros, F cannot be normalized, and the total magnetization density is not conserved.

From (7) we see that the Larmor frequency is determined uniquely by the linear Zeeman effect p , which is totally different from the case of negative quadratic Zeeman effect discussed later. The polar angle defined by (7) is $\arctan(|F_{\perp}|/F_z) = \arctan\left(\sqrt{\frac{-2c_1}{q} \frac{\operatorname{sn}(\xi, \lambda)}{\operatorname{dn}(\xi, \lambda)}}\right)$; its evolution is shown in Fig. 2. It is clear that if $\operatorname{sn}(\xi, \lambda) \neq 0$, then $|F_{\perp}| \neq 0$, and the solution is of axisymmetry-broken phase [28]. However, the region such that $\operatorname{sn}(\xi, \lambda) = 0$ exactly gives the zeros of F , at which the local magnetization vanishes but the order parameter reads

$$\Phi_{\pm 1} = \mp \frac{1}{2} \sqrt{-q/c_1} \operatorname{dn}(\xi, \lambda) e^{i\chi_{\pm 1}}, \quad \Phi_0 = 0, \quad (8)$$

which is of polar phase. Therefore we can confirm that the zeros of $\operatorname{sn}(\xi, \lambda)$ are just the topological defects of the spinor gas, which corresponds to the unmagnetized areas that constitute the periodic DWs when $q \neq 2/\delta$ ($\lambda \neq 1$). Figure 3 displays the spatial distribution of F_x, F_y, F_z , where the intersection points of the three curves in Fig. 3 give the topological defects.

Figure 4 shows the spin configuration determined by (4). Figure 4(a) is the space-time surface of the spin density

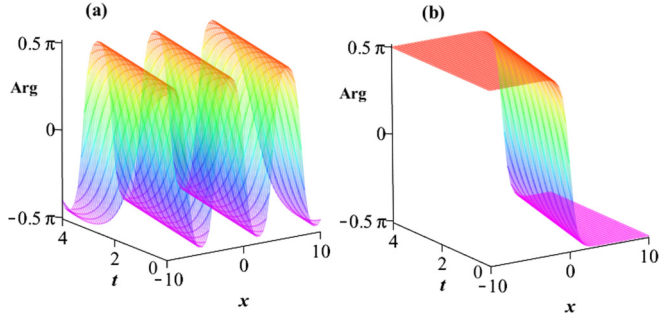


FIG. 2. (Color online) Evolution of the polar angle determined by solution (4): (a) $q = 2$, the periodic case; (b) $q = \frac{430}{217}$ ($\lambda = 1$), the soliton case. The other parameters are $x \in [-10, 10]$, $t \in [0, 3]$, $p = 1$, $c_0 = 216$, $c_1 = -1$, $k_1 = 1$.

vector F (for ^{87}Rb). The color is assigned by the value of F_z , which distinguishes the different magnetization, where the point O corresponds to the zeros of F that indicate the topological defects. Figure 4(b) shows the space-time evolution of the transverse magnetization vector F_\perp , where the lengths of the arrows are $|F_\perp|$, and the color corresponds to that in Fig. 4(a). The heavy yellow and pink regions correspond to the neighbor of the north pole and south pole in Fig. 4(a), respectively. In such regions, the net magnetization $|F_z|$ reaches its maximum value. The regions between the light-green and light-blue lines between the yellow and pink regions are the unmagnetized areas, i.e., the topological defects, corresponding to the point O . The blue curve in Fig. 4(a) presents the spatial evolution of F at $t = 1$. When $q \neq 2/\delta$, along the curve, the spin vector F evolves periodically in the sequence $P \rightarrow O \rightarrow Q \rightarrow O \rightarrow P$, which shows that O actually corresponds to the periodic DWs. Correspondingly, in Fig. 4(b), the color changes in the following sequence: green \rightarrow yellow \rightarrow green \rightarrow blue \rightarrow pink \rightarrow blue \rightarrow pink \rightarrow blue \rightarrow green \rightarrow yellow \rightarrow green. Figure 4(c) gives the spatial formation of the spin vector F along the condensates at $t = 1$, indicating that the topological defects constitute the periodical Bloch-like DWs for the stripe domain. However, at time such that $\sin(pt) = 0$, all spin vectors lie in the $x - z$ plane. The solution presents

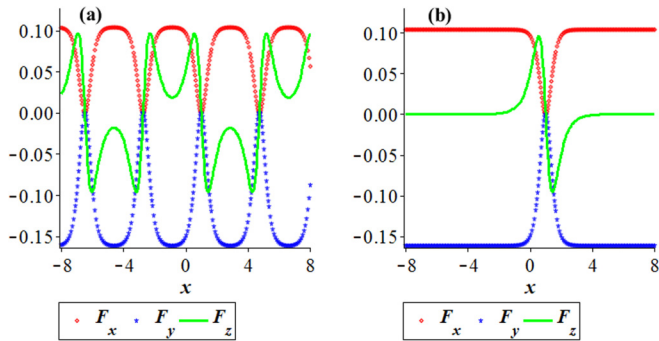


FIG. 3. (Color online) The spatial distribution of F_x, F_y, F_z and topological defects: (a) the periodic case ($q = 2$), the common zeros of the three curves are the topological defects; (b) the soliton case ($q = \frac{430}{217}$), the only common zero of the three curves indicates the topological defect. The other parameters are $p = 1$, $c_1 = -1$, $c_0 = 216$, $k_1 = 1$, $t = 1$, $x \in [-8, 8]$.

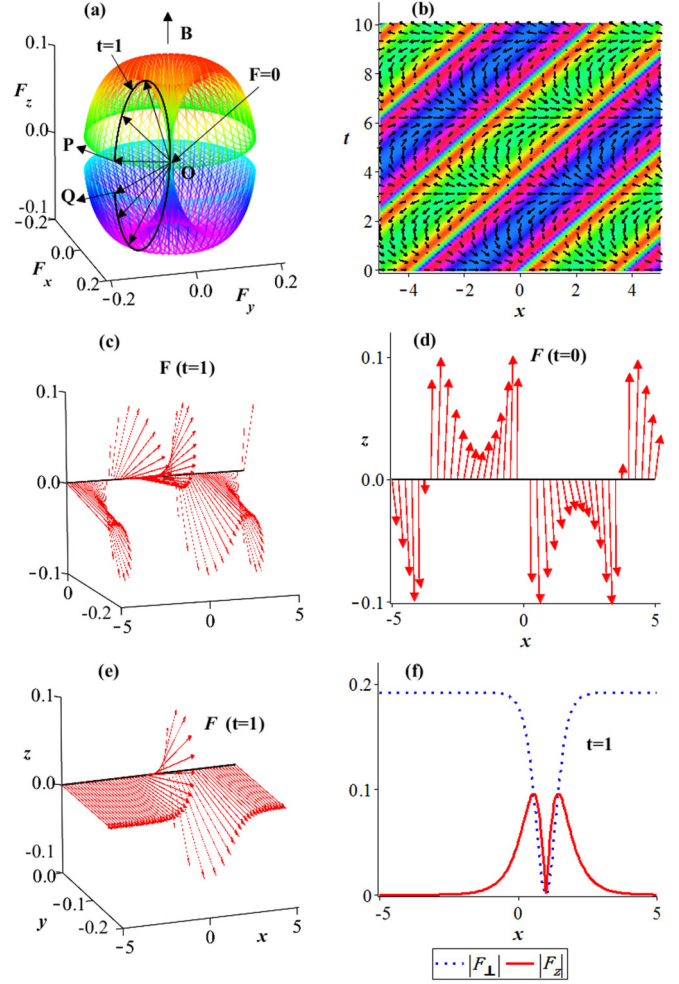


FIG. 4. (Color online) Inhomogeneous spin structure and topological defects induced by positive quadratic Zeeman effect q . (a) The space-time evolution of the spin density vector F , the point O corresponds to topological defects. (b) The field plot of the transverse magnetization vector F_\perp , the green and blue lines between the yellow and pink regions correspond to the evolution of the topological defects. In (a) and (b), $t \in [0, 10]$. (c) The spatial spin configuration at $t = 1$, and (d) the spatial spin configuration at $t = 0$. In (c) and (d), the periodic domain walls are the topological defects. (e) The spatial spin configuration of local magnetism (the soliton case) at $t = 1$, where the unique domain wall is the topological defect. (f) The spatial distribution of $|F_\perp|$ and $|F_z|$ of local magnetism (the soliton case) at $t = 1$, where the only common zero of the two curves indicates the topological defect. In (a)-(d), $q = 2$; in (e) and (f), $q = \frac{430}{217}$ ($\lambda = 1$). The other parameters are $x \in [-5, 5]$, $k_1 = 1$, $c_1 = -1$, $c_0 = 216$, $p = 1$.

helical domain formation with periodic Néel-like DWs formed by the unmagnetized atoms, as shown in Fig. 4(d). Such two kinds of DWs in Figs. 4(c) and 4(d) can be converted to each other periodically. In this case, as $|F_\perp|$ and F_z have common periodic zeros, the transverse ferromagnetic domains are divided by the topological defects periodically. This features agree with the experimental observation for a ^{87}Rb spinor BEC reported in [3]. However, in the experiment, the transverse ferromagnetic domains are formed from nearly pure spinor BEC prepared in the unmagnetized ($m_F = 0$)

phase for $q \gg 2/\delta$ at the beginning, and then rapidly quenched the gas to conditions $q \ll 2/\delta$. Our discussion shows that for q around $2/\delta$, a similar phenomenon should also be observed.

It is remarkable that when $q = 2/\delta$ ($\lambda = 1$), (4) gives a novel superposition solitonlike solution:

$$\begin{aligned}\Phi_{\pm 1} &= [\sqrt{-c_1/(c_0 - c_1)} \tanh(\xi) \mp \sqrt{2/\delta} \operatorname{sech}(\xi)] e^{i\chi_{\pm 1}}, \\ \Phi_0 &= \tanh(\xi) e^{i\chi_0}.\end{aligned}$$

The shape of such solutions are determined by the ratio $\gamma = |c_0/c_1|$. For ^{87}Rb , $\gamma \gg 1$, each $|\Phi_{\pm 1}|^2$ behaves like a bright soliton. This fact implies that $q = 2/\delta$ is an unstable point of dynamical phase transition. As we usually have $|c_1| \ll c_0$, $q = 2/\delta$ can be compared with the quantum phase transition point $\bar{q} = 2|\bar{c}_1|n$ (i.e., $q = 2$) mentioned in [3]. In this case, we have

$$\begin{aligned}|F_{\perp}| &= \sqrt{-8c_1/(c_0 - c_1)} \tanh^2(\xi), \\ F_z &= 2\sqrt{q/(c_0 - c_1)} \tanh(\xi) \operatorname{sech}(\xi).\end{aligned}\quad (9)$$

The atom exchange between the sublevels is small near the soliton propagation direction, which permits only a unique spin DW. Far away from this region, the atom exchange of the component $m_F = \pm 1$ is almost uniform, which gives no net magnetization. Therefore the net magnetization is concentrated in a local range, as shown in Figs. 4(e) and 4(f).

When $|F_{\perp}| \neq 0$, the $\text{SO}(2)$ symmetry is broken in the direction of the transverse magnetization. In our solution, the transverse magnetization is nonuniform, i.e., it is space- and time-dependent, which causes the inhomogeneous symmetry breaking in the spin evolution. To investigate the symmetry of the order parameters in spin space, we give the visualized realization of the order parameter for $q > 0$ in the spin space. Because an integer-spin state can be described in terms of the spherical harmonics $Y_f^m(\hat{s})$ [$\hat{s} = (\alpha, \beta)$, α is taken as the polar (colatitude) coordinate with $\alpha \in [0, \pi]$, and $\beta \in [0, 2\pi]$ is the azimuthal (longitudinal) coordinate], the above order parameter can be visualized by drawing the wave functions in spin space by the surface of $|\Psi(\hat{s})|^2$, where $\Psi(\hat{s}) = \Phi_{+1}Y_1^1(\hat{s}) + \Phi_0Y_1^0(\hat{s}) + \Phi_{-1}Y_1^{-1}(\hat{s})$.

In mathematics, spherical harmonics are the angular portion of a set of solutions to Laplace's equation. Represented in a system of spherical coordinates, Laplace's spherical harmonics $Y_f^m(\hat{s})$ are a specific set of spherical harmonics that forms an orthogonal system.

Figure 5 shows spatial variation of the order parameter in a unit cell visualized by plotting a surface with spherical coordinates, where the color represents the phase, i.e., the argument $\arg \Psi(\hat{s})$ [16], which is defined on $[-\pi, \pi]$. It displays that the spin states of the order parameter in the spin space is space-time pointwise different. As a comparison, Figs. 5(a) and 5(b) are the spin states for the same position and quadratic Zeeman effect but different time, whereas Figs. 5(a) and 5(c) are for the same position and time but different quadratic Zeeman effect. One can see that for the order parameters for states (a) and (b), they not only differ in their orientations, but also have different morphologies near the centers, so they cannot be identified in the spin space via a rotation, which is quite different from the case discussed in [16] for ground state. Figures 5(a) and 5(c) show that the change of the quadratic Zeeman effect will change the spin

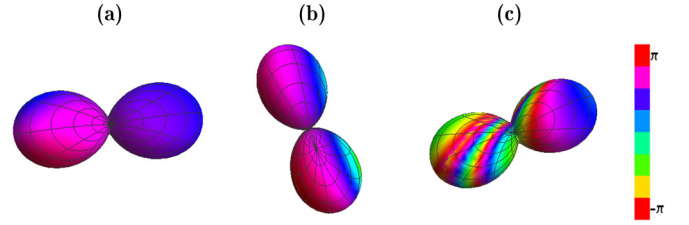


FIG. 5. (Color online) Inhomogeneity of the order parameter ($\Phi_{-1}, \Phi_0, \Phi_1$) in the spin space determined by the positive quadratic Zeeman effect. As a comparison for the spin state, (a) and (b) are for the same position ($x = 4$) and quadratic Zeeman effect ($q = 3$) but different time: $t = 2$ in (a), $t = 4.5$ in (b); (a) and (c) are for the same position ($x = 4$) and time ($t = 2$) but different quadratic Zeeman effect: $q = 3$ in (a), $q = 9$ in (c). The other parameters are taken as $p = 1, k_1 = 1, c_1 = -1, c_0 = 216$. Notice that the three figures have different morphologies near the centers, so they cannot be identified in the spin space via a rotation.

state of the order parameter. This implies that the presence of the quadratic Zeeman effect can lead to different morphology for the space-time-dependent spin state.

We now turn to the population distribution determined by solution (4) and recall a conclusion in mathematics: for a continuous function $f(t)$ with period T , we have $\int_0^T f(x)dx = \int_c^{T+c} f(x)dx = \int_0^T f(x+c)dx$ for any constant c . By this fact, we see that within a period, the atom number, $N_m = \int_0^T |\Phi_m[k(x + k_1t)]|^2 dx = \int_{kk_1t}^{T+kk_1t} |\Phi_m(kx)|^2 dx = \int_0^T |\Phi_m(kx)|^2 dx$ ($m = \pm 1, 0$), of each component is time-independent; therefore we confirm that the population exchange between the $m_F = \pm 1$ and $m_F = 0$ components is in an equilibrium state.

IV. TOPOLOGICAL DEFECTS AND INHOMOGENEOUS SPIN BY NEGATIVE QUADRATIC ZEEMAN EFFECT

For a negative quadratic Zeeman effect, exact solutions are obtained for both ferromagnetic ($c_1 = -1$) and antiferromagnetic ($c_1 = 1$) interactions when $|c_1| < c_0$. Set $\nu = -2q/(c_0 - c_1)$ and $k = \sqrt{(c_0 + c_1)A_{-1}^2}$, and Eq. (1) has the solution

$$\begin{aligned}\Phi_{\pm 1} &= A_{\pm 1} \operatorname{sn}(\xi, \lambda) e^{i\chi_{\pm 1}}, \\ \Phi_0 &= \sqrt{-2A_1 A_{-1}} \operatorname{cn}(\xi, \lambda) e^{i\chi_0},\end{aligned}\quad (10)$$

where k_1, A_{-1} are free parameters, $A_1 = \sqrt{\nu} - A_{-1}$, $\lambda = \sqrt{(c_0 + c_1)\nu}/k$, $\xi = k(x - k_1t)$, $\chi_{\pm 1} = k_1x - \mu_{\pm 1}t$, $\chi_0 = (\chi_1 + \chi_{-1})/2$, with

$$\begin{aligned}\mu_{\pm 1} &= (k_1^2 + k^2)/2 + 2c_0A_{-1}^2 - 2\sqrt{\nu}(c_0 \pm c_1)A_{-1} \\ &\quad \pm c_1\nu \mp p.\end{aligned}$$

Let $t = 0$, $q = 0$, and we get the initial conditions before the quadratic Zeeman effect as

$$\begin{aligned}\Phi_{\pm 1} &= \pm A_1 \sin(kx) e^{ik_1x}, \\ \Phi_0 &= \sqrt{2}A_1 \cos(kx) e^{ik_1x},\end{aligned}\quad (11)$$

which is of a polar phase, where k, k_1 are arbitrary constants. The initial state ($t = 0$) of solution (10) is shown in Fig. 6.

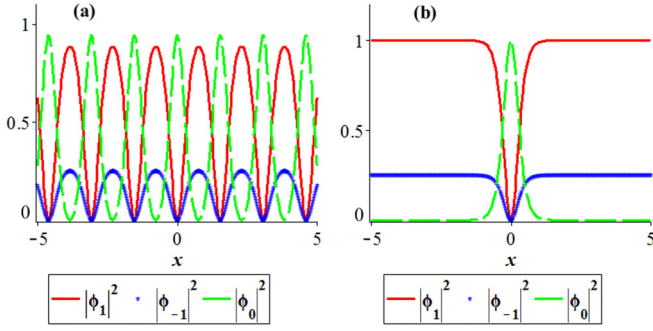


FIG. 6. (Color online) Initial states of $\Phi_{\pm 1}, \Phi_0$ determined by solution (10): (a) $q = -3$, the periodic case; (b) $q = -3.875$ ($\lambda = 1$), the soliton case. The other parameters are $t = 0, x \in [-5, 5], p = 1, c_1 = 1, c_0 = 32, A_{-1} = -0.5, k_1 = 1$.

In general, Eq. (10) indicates a solution of broken-axisymmetry phase, and the spin vector is given by

$$\begin{aligned} F_x &= 2\sqrt{-A_1 A_{-1} \nu} \operatorname{sn}(\xi, \lambda) \operatorname{cn}(\xi, \lambda) \cos \Omega t, \\ F_y &= -2\sqrt{-A_1 A_{-1} \nu} \operatorname{sn}(\xi, \lambda) \operatorname{cn}(\xi, \lambda) \sin \Omega t, \\ F_z &= (\nu - 2\sqrt{\nu A_{-1}}) \operatorname{sn}^2(\xi, \lambda), \end{aligned} \quad (12)$$

where $\Omega = (p - c_1 \nu + 2c_1 A_{-1} \sqrt{\nu})$ gives the Larmor frequency. Different from the case of $q > 0$, the Larmor frequency is not only determined by the linear Zeeman effect but also by the quadratic Zeeman effect. Similar to the case of $q > 0$, the zeros of F determine the topological defects constituted by the unmagnetized atoms.

The expression of solution (10) requires $A_1 A_{-1} \leq 0$. The cases for $A_{-1} > 0$ and $A_{-1} < 0$ are different. One can see that if $A_{-1} > 0, q$ should be restricted in the region $-\frac{1}{2}(c_0 - c_1)A_{-1}^2 \leq q \leq 0$, in this case, while $q = 0$ gives a periodic polar state

$$\begin{aligned} \Phi_{\pm 1} &= \mp A_{-1} \sin(\xi) e^{i\chi_{\pm 1}}, \\ \Phi_0 &= \sqrt{2} A_{-1} \cos(\xi) e^{i\chi_0}, \end{aligned} \quad (13)$$

$q = -A_{-1}^2(c_0 - c_1)/2$ presents a ferromagnetic phase

$$\Phi_0 = \Phi_1 = 0, \quad \Phi_{-1} = A_{-1} \tanh(\xi) e^{i\chi_{\pm 1}}. \quad (14)$$

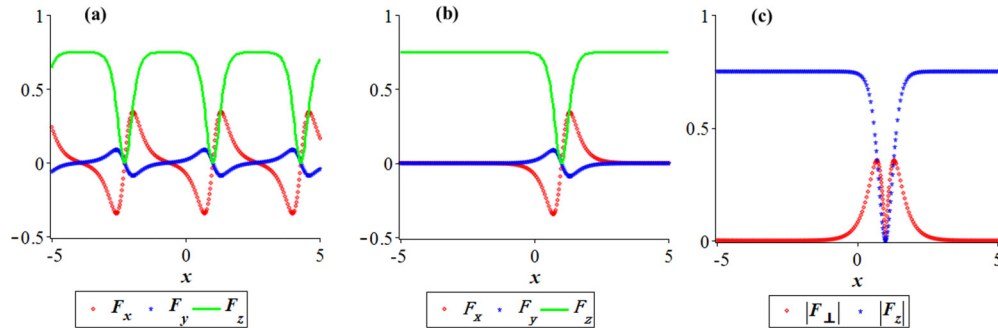


FIG. 7. (Color online) (a) The spatial distribution of F_x, F_y, F_z for $q = -3.87$ (the periodic case), the common zeros of the three curves show the topological defects. (b) The spatial distribution of F_x, F_y, F_z for $q = -3.875$ ($\lambda = 1$) (the soliton case), the only common zero of the three curves indicates the topological defect. (c) The spatial distribution of $|F_{\perp}|$ and $|F_z|$ for $q = -3.875$ ($\lambda = 1$), the only common zero of the two curves is the topological defect. The other parameters are $p = 1, c_1 = 1, c_0 = 32, A_{-1} = -0.5, k_1 = 1, t = 1, x \in [-5, 5]$.

This suggests that by tuning q , it is possible to get polar phase or ferromagnetic phase from the broken-axisymmetry phase, which means that tuning q can change the population in each component.

If $A_{-1} < 0$, no further restriction on q is required. For simplicity, hereafter we only discuss the case for $A_{-1} < 0$. In such a situation, note that $q = -\frac{1}{2}(c_0 - c_1)A_{-1}^2$ gives the soliton state, the order parameter reads

$$\Phi_{\pm 1} = A_{\pm 1} \tanh(\xi) e^{i\chi_{\pm 1}}, \quad \Phi_0 = \sqrt{-2A_1 A_{-1}} \operatorname{sech}(\xi) e^{i\chi_0},$$

and the spin vector becomes

$$\begin{aligned} F_x &= 2\sqrt{-A_1 A_{-1} \nu} \tanh(\xi) \operatorname{sech}(\xi) \cos \Omega t, \\ F_y &= -2\sqrt{-A_1 A_{-1} \nu} \tanh(\xi) \operatorname{sech}(\xi) \sin \Omega t, \\ F_z &= (\nu - 2\sqrt{\nu A_{-1}}) \tanh^2(\xi). \end{aligned}$$

Figures 7(a)–7(c) display the spatial distribution of F_x, F_y, F_z and $|F_{\perp}|, |F_z|$, respectively. Similar to Figs. 3(a) and 3(b), the intersection points of the three curves in Figs. 7(a) and 7(b) give the topological defects. In the soliton case, both the atom exchange between the sublevels and the net magnetization vanish on the topological defects. However, the transverse magnetization is concentrated on the region near the defect, and far away from this region, it becomes zero but F_z reaches its maximum, which gives a uniform net magnetization with no population exchange, as Fig. 7(c) displays. This is contrary to the case of solution (4) shown in Fig. 4(f). Roughly speaking, for the shapes of the curves in Fig. 7(c) and Fig. 4(f), there is an exact interchange between the distribution of $|F_{\perp}|$ and $|F_z|$. On the other hand, it is the same as the case of $q > 0$, for solution (10). The zeros of $\operatorname{sn}(\xi, \lambda)$ present the topological defects, and at these defects, the order parameter becomes $\Phi_{\pm 1} = 0, \Phi_0 = \sqrt{-2A_1 A_{-1}} e^{i\chi_0}$, which is of polar phase, but besides them, the order parameter is of axisymmetry-broken phase.

The evolution of the polar angle determined by solution (10) is shown in Fig. 8. Similar to the case of $q > 0$, the population of each component is also conserved within a period, and the atom exchange between the sublevels is also in an equilibrium state. However, the spin configuration for the case of $q < 0$ is rather different from the case of $q > 0$. First, the Larmor frequency is not only determined by the linear Zeeman effect, but also by the quadratic Zeeman effect. In addition, the spin domain formation is completely different. We show the spin

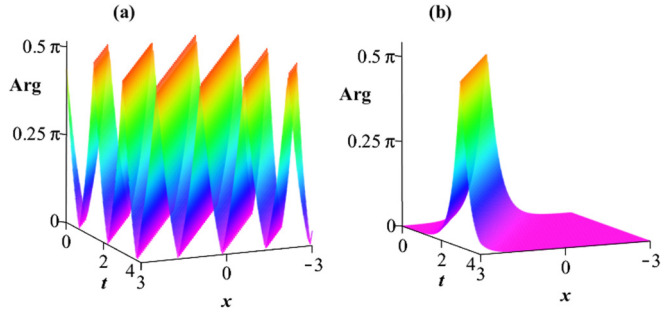


FIG. 8. (Color online) Evolution of the polar angle determined by solution (10): (a) $q = -3$, the periodic case; (b) $q = -\frac{31}{8}$ ($\lambda = 1$), the soliton case. The other parameters are $x \in [-3, 3]$, $t \in [0, 3]$, $p = 1$, $c_1 = 1$, $c_0 = 32$, $k_1 = 1$, $A_{-1} = -0.5$.

domain formation determined by solution (10) in Fig. 9 to compare with Fig. 4. One can find that Figs. 9(a) and 9(c) present different spin patterns compared with that shown in Figs. 4(c) and 4(e). Figure 9(a) is the spatial spin configuration, and its spin DWs are of Bloch-like type. Figure 9(b) shows the spin configuration at the time such that $\sin(\Omega t) = 0$. In this case, all spin vectors have almost the same direction and lie in the $x - z$ plane and the topological defect does not form domain walls, although they divided the domain into subdomains periodically, which is very different from the case shown in Fig. 4(d).

Taking ^{23}Na ($c_1 = 1$) as an example (for $c_1 = -1$, such as ^{87}Rb , the result is similar), Fig. 10(a) gives the spin density surface. Compared with the case of $q > 0$, it has a different topological structure. Figure 10(b) shows how the negative quadratic Zeeman effect affects the intensity of F , F_{\perp} , and F_z . The black curve in Fig. 10(a) shows the spatial evolution of F at $t = 1$. Along the curve, one cycle movement corresponds to one period of the spin domain. Similar to the case of $q > 0$, the nonuniform periodic population distribution and exchange bring on the periodic spin DWs formed by the topological defects, which is indicated by point O . In addition, the center areas of a spin domain correspond to the north poles in Fig. 10(a), where $F_{\perp} = 0$, and no population exchange between the sublevels occurs. In such areas, the spin reaches its maximum net magnetization.

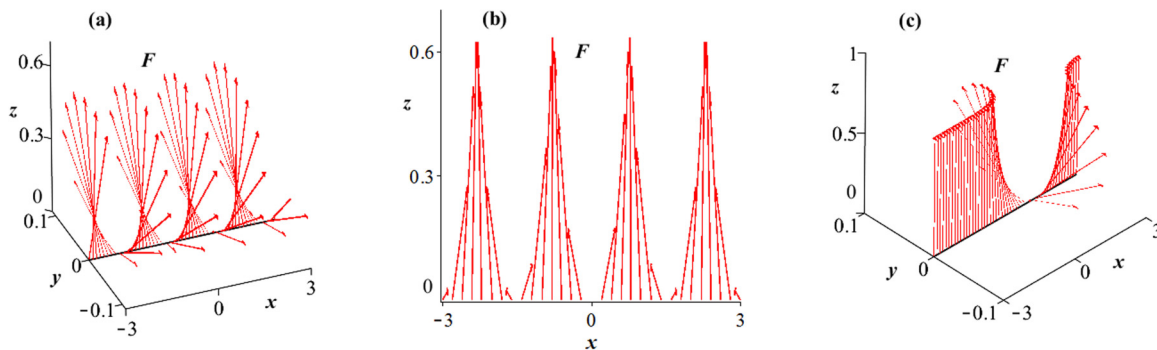


FIG. 9. (Color online) Inhomogeneous spin structure and the topological defects determined by solution (10) for different t and q : (a) the spatial spin configuration at $t = 1$ for $q = -3$, the periodic case; (b) the spatial spin configuration at $t = 0$ for $q = -3$; and (c) the spatial spin configuration at $t = 1$ for $q = -\frac{31}{8}$ ($\lambda = 1$), the soliton case. The other parameters are: $x \in [-3, 3]$, $p = 1$, $c_1 = 1$, $c_0 = 32$, $k_1 = 1$, $A_{-1} = -0.5$. The domain walls are formed by the topological defects.

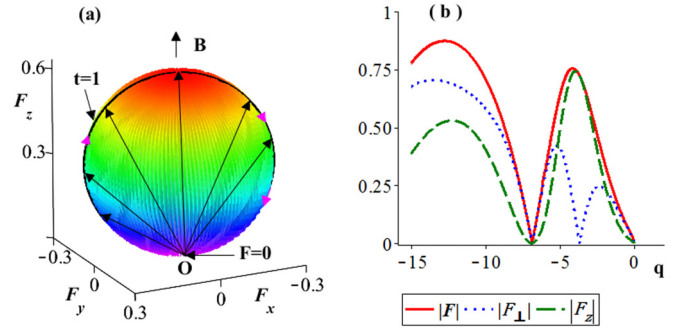


FIG. 10. (Color online) Inhomogeneous spin structure induced by negative quadratic Zeeman effect: (a) the space-time evolution of the spin density vector F , the color indicates the intensity of F_z ; (b) the influence of q on F , F_{\perp} and F_z . In (a), $p = 1$, $q = -3$, $x \in [-5, 5]$, $t \in [0, 15]$; in (b), $x = 0$, $t = 1$, $q \in [-15, 0]$. The other parameters are $A_{-1} = -0.5$, $p = 1$, $k_1 = 1$, $c_1 = 1$, $c_0 = 32$.

Experimentally, $q < 0$ can be reached by using a bias magnetic field B and a microwave dressing field M . Let q_B be the quadratic Zeeman shift given by B and q_M be the quadratic energy shift due to the ac Stark shift caused by M , q can be tuned by virtue of $q = q_B + q_M$. In the recent experiment [4], in a quasi-1D case, with up to 3×10^6 sodium atoms with a peak atom density of $n_0 = 5.4 \times 10^{14} \text{ cm}^{-3}$, in an optical dipole trap, under a bias magnetic field $B = 97 \text{ mG}$, by using microwave powers between 0 and 7.5 W, the quadratic Zeeman effect can be tuned between $q_B = h \times 2.5 \text{ Hz}$ to -18.5 Hz . By rapidly switching the quadratic Zeeman effect from positive to negative values, the dynamics of an antiferromagnetic sodium BEC quenched across a quantum phase transition has been observed. However, the phase coherence between the dynamically created $m_F = \pm 1$ spin components in relation to topological defect formation was not explored. The above analytical solution for $q < 0$ provides a precise description for possible dynamics of this experiment and shows further that the same dynamics could be observed for the ^{87}Rb BEC. By probing the Larmor precession [63], the novel features are expected to be tested.

It is found that tuning the linear Zeeman effect and quadratic Zeeman effect will cause a pointwise-different influence to the spin dynamics. Taking ^{87}Rb and ^{23}Na as examples,

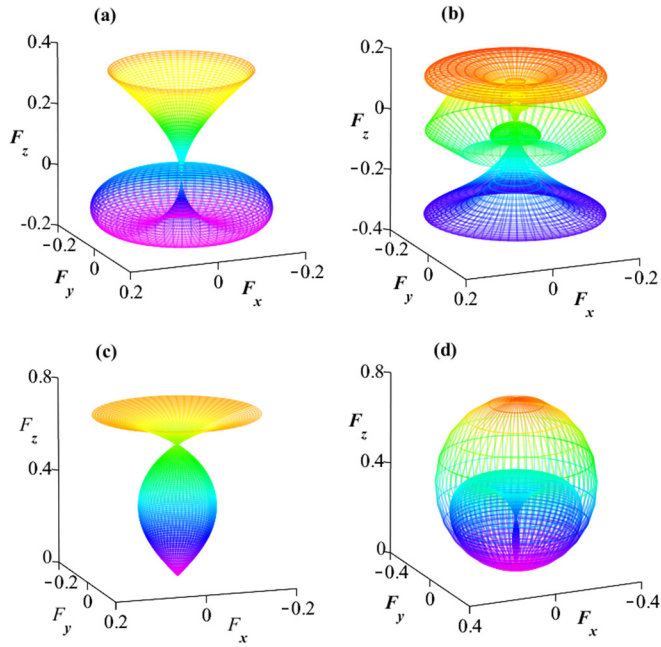


FIG. 11. (Color online) Pointwise evolution of the spin density vector F in the linear and quadratic Zeeman effects p and q at the same time ($t = 1$) but different position, the color indicates the intensity of F_z : (a, b) for $q > 0$, where $x = 2$ in (a), $x = 3.3$ in (b), $q \in [0, 10]$; (c, d) for $q < 0$, where $x = 1.7$ in (c), $x = 2.7$ in (d), $q \in [-3.87, 0]$, $A_{-1} = -0.5$. In both cases $p \in [0, 2\pi], k_1 = 1$.

Figs. 11(a) and 11(b) show the pointwise evolution of F in p and q for $q > 0$; Figs. 11(c) and 11(d) are for $q < 0$. These figures clearly show the inhomogeneous influence of the Zeeman effects on the spin structures.

V. CONCLUSION

In conclusion, in the presence of the positive and negative quadratic Zeeman effect, respectively, we obtain two exact solutions of broken-axisymmetry phase for spin-1 BEC. Two kinds of inhomogeneous spin patterns are displayed, the magnetization dynamics dominated by the quadratic Zeeman effect are discussed in detail, and the topological defects are described analytically. Our results provide an alternate prospect for spin configuration in spin-1 BEC, and similar phenomena are expected to be found also in spin-2 BEC. We will discuss this topic in another paper.

ACKNOWLEDGMENTS

This work was supported by the NKBRSCF under Grants No. 2011CB921502 and No. 2012CB821305; the NSFC under Grants No. 11475073, No. 11325417, No. 11174115, No. 61227902, No. 61378017, and No. 11434015; the SKLQOQOD under Grant No. KF201403; the SPRPCAS under Grant No. XDB01020300; and the NSF of Hebei Province of China under Grant No. A2012202022.

-
- [1] J. Stenger, S. Inouye, D. M. Stamper-Kurn, H.-J. Miesner, A. P. Chikkatur, and W. Ketterle, *Nature (London)* **396**, 345 (1998).
- [2] D. M. Stamper-Kurn, M. R. Andrews, A. P. Chikkatur, S. Inouye, H.-J. Miesner, J. Stenger, and W. Ketterle, *Phys. Rev. Lett.* **80**, 2027 (1998).
- [3] L. Sadler, J. M. Higbie, S. R. Leslie, M. Vengalattore, and D. M. Stamper-Kurn, *Nature (London)* **443**, 312 (2006).
- [4] E. M. Bookjans, A. Vinit, and C. Raman, *Phys. Rev. Lett.* **107**, 195306 (2011).
- [5] T.-L. Ho, *Phys. Rev. Lett.* **81**, 742 (1998).
- [6] T. Ohmi and K. Machida, *J. Phys. Soc. Jpn.* **67**, 1822 (1998).
- [7] C. K. Law, H. Pu, and N. P. Bigelow, *Phys. Rev. Lett.* **81**, 5257 (1998).
- [8] H. Pu, C. K. Law, S. Raghavan, J. H. Eberly, and N. P. Bigelow, *Phys. Rev. A* **60**, 1463 (1999).
- [9] F. Zhou, *Phys. Rev. Lett.* **87**, 080401 (2001).
- [10] E. Demler and F. Zhou, *Phys. Rev. Lett.* **88**, 163001 (2002).
- [11] W. Zhang, S. Yi, and L. You, *New J. Phys.* **5**, 77 (2003).
- [12] I. Bloch, J. Dalibard, and W. Zwerger, *Rev. Mod. Phys.* **80**, 885 (2008).
- [13] L. Zhou, H. Pu, H. Y. Ling, and W. P. Zhang, *Phys. Rev. Lett.* **103**, 160403 (2009).
- [14] Z. Cai, X. F. Zhou, and C. J. Wu, *Phys. Rev. A* **85**, 061605(R) (2012).
- [15] D. M. Stamper-Kurn and M. Ueda, *Rev. Mod. Phys.* **85**, 1191 (2013).
- [16] M. Ueda and Y. Kawaguchi, *Phys. Rep.* **520**, 253 (2012).
- [17] M. Ueda, *Annu. Rev. Condens. Matter Phys.* **3**, 263 (2012).
- [18] P. G. Kevrekidis, G. Theocharis, D. J. Frantzeskakis, and B. A. Malomed, *Phys. Rev. Lett.* **90**, 230401 (2003).
- [19] F. K. Abdullaev, J. G. Caputo, R. A. Kraenkel, and B. A. Malomed, *Phys. Rev. A* **67**, 013605 (2003).
- [20] V. N. Serkin, A. Hasegawa, and T. L. Belyaeva, *Phys. Rev. Lett.* **98**, 074102 (2007).
- [21] G. Juzeliunas, J. Ruseckas, P. Ohberg, and M. Fleischhauer, *Lith. J. Phys.* **47**, 351 (2007).
- [22] V. N. Serkin, A. Hasegawa, and T. L. Belyaeva, *Phys. Rev. A* **81**, 023610 (2010).
- [23] M. J. Edmonds, M. Valiente, G. Juzeliunas, L. Santos, and P. Ohberg, *Phys. Rev. Lett.* **110**, 085301 (2013).
- [24] P. O. Fedichev, Yu. Kagan, G. V. Shlyapnikov, and J. T. M. Walraven, *Phys. Rev. Lett.* **77**, 2913 (1996).
- [25] M. Theis, G. Thalhammer, K. Winkler, M. Hellwig, G. Ruff, R. Grimm, and J. H. Denschlag, *Phys. Rev. Lett.* **93**, 123001 (2004).
- [26] D. J. Papoular, G. V. Shlyapnikov, and J. Dalibard, *Phys. Rev. A* **81**, 041603(R) (2010).
- [27] H. Saito and M. Ueda, *Phys. Rev. A* **72**, 023610 (2005).
- [28] K. Murata, H. Saito, and M. Ueda, *Phys. Rev. A* **75**, 013607 (2007).
- [29] D. Jacob, L. X. Shao, V. Corre, T. Zibold, L. De Sarlo, E. Mimoun, J. Dalibard, and F. Gerbier, *Phys. Rev. A* **86**, 061601(R) (2012).
- [30] L. Santos, M. Fattori, J. Stuhler, and T. Pfau, *Phys. Rev. A* **75**, 053606 (2007).

- [31] S. Uchino, M. Kobayashi, and M. Ueda, *Phys. Rev. A* **81**, 063632 (2010).
- [32] J. Kronjäger, C. Becker, P. Soltan-Panahi, K. Bongs, and K. Sengstock, *Phys. Rev. Lett.* **105**, 090402 (2010).
- [33] D. R. Romano and E. J. V. de Passos, *Phys. Rev. A* **70**, 043614 (2004).
- [34] J. Kronjäger, C. Becker, M. Brinkmann, R. Walser, P. Navez, K. Bongs, and K. Sengstock, *Phys. Rev. A* **72**, 063619 (2005).
- [35] C. J. Tao, Z. R. Jiao, and Q. Gu, *Phys. Rev. A* **79**, 043614 (2009).
- [36] N. T. Phuc, Y. Kawaguchi, and M. Ueda, *Phys. Rev. A* **84**, 043645 (2011).
- [37] J. Guzman, G. B. Jo, A. N. Wenz, K. W. Murch, C. K. Thomas, and D. M. Stamper-Kurn, *Phys. Rev. A* **84**, 063625 (2011).
- [38] J. D. Sau, S. R. Leslie, M. D. Cohen, and D. M. Stamper-Kurn, *New J. Phys.* **12**, 085011 (2010).
- [39] M. Matuszewski, *Phys. Rev. Lett.* **105**, 020405 (2010).
- [40] S. R. Leslie, J. Guzman, M. Vengalattore, J. D. Sau, M. L. Cohen, and D. M. Stamper-Kurn, *Phys. Rev. A* **79**, 043631 (2009).
- [41] B. Damski and W. H. Zurek, *Phys. Rev. Lett.* **99**, 130402 (2007).
- [42] K. Rodríguez, A. Argüelles, A. K. Kolezhuk, L. Santos, and T. Vekua, *Phys. Rev. Lett.* **106**, 105302 (2011).
- [43] M. Scherer, B. Lucke, G. Gebreyesus, O. Topic, F. Deuretzbacher, W. Ertmer, L. Santos, J. J. Arlt, and C. Klempt, *Phys. Rev. Lett.* **105**, 135302 (2010).
- [44] T. Isoshima and S. Yip, *J. Phys. Soc. Jpn.* **75**, 074605 (2006).
- [45] F. Gerbier, A. Widera, S. Fölling, O. Mandel, and I. Bloch, *Phys. Rev. A* **73**, 041602 (2006).
- [46] W.-J. Huang and S.-C. Gou, *Phys. Rev. A* **59**, 4608 (1999).
- [47] T. P. Meyrath, F. Schreck, J. L. Hanssen, C.-S. Chuu, and M. G. Raizen, *Phys. Rev. A* **71**, 041604(R) (2005).
- [48] A. L. Gaunt, T. F. Schmidutz, I. Gotlibovych, R. P. Smith, and Z. Hadzibabic, *Phys. Rev. Lett.* **110**, 200406 (2013).
- [49] M. Olshanii, *Phys. Rev. Lett.* **81**, 938 (1998).
- [50] H. E. Nistazakis, D. J. Frantzeskakis, P. G. Kevrekidis, B. A. Malomed, and R. Carretero-Gonzalez, *Phys. Rev. A* **77**, 033612 (2008).
- [51] M.-S. Chang, C. D. Hamley, M. D. Barrett, J. A. Sauer, K. M. Fortier, W. Zhang, L. You, and M. S. Chapman, *Phys. Rev. Lett.* **92**, 140403 (2004).
- [52] A. Lamacraft, *Phys. Rev. Lett.* **98**, 160404 (2007).
- [53] A. T. Black, E. Gomez, L. D. Turner, S. Jung, and P. D. Lett, *Phys. Rev. Lett.* **99**, 070403 (2007).
- [54] H. Saito, Y. Kawaguchi, and M. Ueda, *Phys. Rev. A* **75**, 013621 (2007).
- [55] J. D. Sau, S. R. Leslie, D. M. Stamper-Kurn, and M. L. Cohen, *Phys. Rev. A* **80**, 023622 (2009).
- [56] R. Barnett, A. Polkovnikov, and M. Vengalattore, *Phys. Rev. A* **84**, 023606 (2011).
- [57] Y. Wu, *Phys. Rev. A* **54**, 4534 (1996).
- [58] J. Ieda, T. Miyakawa, and M. Wadati, *Phys. Rev. Lett.* **93**, 194102 (2004); *J. Phys. Soc. Jpn.* **73**, 2996 (2004); *Laser Phys.* **16**, 678 (2006).
- [59] M. Uchiyama, J. Ieda, and M. Wadati, *J. Low. Temp. Phys.* **148**, 399 (2007).
- [60] L. Li, Z. D. Li, B. A. Malomed, D. Mihalache, and W. M. Liu, *Phys. Rev. A* **72**, 033611 (2005).
- [61] R. Beals and R. Wong, *Special Functions* (Cambridge University Press, Cambridge, UK, 2010).
- [62] H. E. Salzer, *Comm. ACM* **5**, 399 (1962).
- [63] J. M. Higbie, L. E. Sadler, S. Inouye, A. P. Chikkatur, S. R. Leslie, K. L. Moore, V. Savalli, and D. M. Stamper-Kurn, *Phys. Rev. Lett.* **95**, 050401 (2005).